

Modelling of the droplet entrainment phenomena for the simulation of reflood phase during a large-break loss-of-coolant accident in a pressurized water reactor

Jeon Min Yoo, Byong Jo Yun, Jae Jun Jeong*

School of Mechanical Engineering, Pusan National University (PNU)

*Corresponding author: jjjeong@pusan.ac.kr

1. Introduction

The droplet has a large surface area per unit volume and so it has excellent heat transfer characteristics. In a large-break loss-of-coolant (LOCA) in a pressurized water reactor (PWR), droplet behavior in the reactor core is very important. In particular, the droplets downstream of the quench front (QF) during the reflood phase greatly affect the thermal-hydraulic phenomena inside the reactor core. The droplets reduce the temperature of the superheated vapor through interfacial heat transfer and evaporate near the fuel to increase wall heat transfer. That is, the droplet behavior downstream of the QF is closely related to the prediction of fuel temperature. The droplets entrained into the U-tubes induce the so-called steam binding effect, which also affects the core heat removal.

Downstream of the QF, a post-dryout regime (inverted flow) is formed. To observe the thermal-hydraulic behavior under this flow condition, visualization experiments have been conducted[1-5]. Through the experiments, various droplet entrainment mechanisms in the post-dryout regime were identified. However, a few studies have been conducted to develop the droplet entrainment model using the experimental observation results. And there are still insufficient experimental and theoretical researches related to the droplet entrainment phenomena downstream of the QF.

In this paper, a droplet entrainment model was proposed based on the results of the experiments observing the droplet entrainment phenomena in post-dryout regime. The proposed model and the existing models[6-9] were implemented into the CUPID code [10], in which the 3-field model is applied. And they were evaluated using reflood heat transfer experiments, such as FLECHT SEASET [11] and FEBA [12].

2. Existing droplet entrainment models

The COBRA-TF, a subchannel analysis code, has used a droplet entrainment model in which the gas mass flow rate is multiplied by several engineering factors(Table I). This model has been applied in the reflood analysis for a long time. In the study of Valette et al.[9], reflood heat transfer experiments were simulated using the CATHARE3 code, in which the entrainment model based on relative velocity of gas and liquid was applied. The models used in both codes contain several engineering factors(Table I), but the problem is that the basis of these factors is not clear. Holowach et al.[8] developed a model to predict the

amount of droplets generated at the QF using Kelvin-Helmholz instability analysis and data of vertical pipe reflood experiments. However, it remains to be questioned whether the assumptions and experimental data used in the model development adequately reflected the droplet entrainment phenomena of the rod bundle condition.

Table I: Existing droplet entrainment correlations

	Correlations
COBRA-TF	$m_E = \min[1.0, 5.0\alpha_l] \times \max[0.0, m_{E1} - \max(0.0, m_{d,i})]$ $m_{E1} = 1.5 \min \left[2.5, \left(\frac{u_g}{u_{crit}} \right)^2 \right] m_g$ $u_{crit} = \left(\frac{4We_d}{3C_D} \right)^{0.25} \left(\frac{\sigma g \Delta \rho}{\rho_g^2} \right)^{0.25}$
Yonamoto	$u_{crit} = \left(\frac{3.57}{C_D \alpha_l} \right) \left(\frac{\sigma g \Delta \rho}{\rho_g^2} \right)^{0.25} N_{\mu g}^{1/6}$ $N_{\mu g} = \frac{\mu_g}{\left(\rho_g \sigma \sqrt{\frac{\sigma}{g \Delta \rho}} \right)^{0.5}}$
CATHARE3	$m_E = 4 \times 10^{-6} A_{i,l} \rho_l (u_g - u_l) We^{0.625}$ $We = \frac{\rho_g (u_g - u_l)^2 D_h}{\sigma}$
Holowach	$m_E = 1.46 \times 10^{-8} \frac{\lambda_{crit} \rho_l P_h (u_{g,crit}^2 + u_{g,bqf}^2)^{0.5}}{A_f} Re_{g,gen}^{1.83}$

3. Modelling of the droplet entrainment phenomena

3.1. Droplet entrainment phenomena in the post-dryout regime

Ishii[2-4], Jarlais[1], Babbelli[5] performed the visualization experiments to understand the thermal-hydraulic behavior in the post-dryout regime. They observed the post-dryout flow under adiabatic and diabatic conditions using Freon-113. As a results of the experiments, the post-dryout flow was divided into an inverted annular flow, agitated regime, and dispersed droplet regime. Under the inverted annular flow conditions, droplets were produced on the core liquid jet through varicose jet breakup, sinuous jet breakup(Fig. 1) and roll-wave entrainment. In the agitated region formed downstream of the inverted

annular flow, droplets were generated from the core liquid jet and the liquid sheet located near the heating surface (Fig. 1). The dispersed droplet regime consisted of multiple droplets and a small amount of liquid ligament. Through these, it can be seen that droplets are mainly entrained from the core liquid jet and liquid sheet in the post-dryout regime.

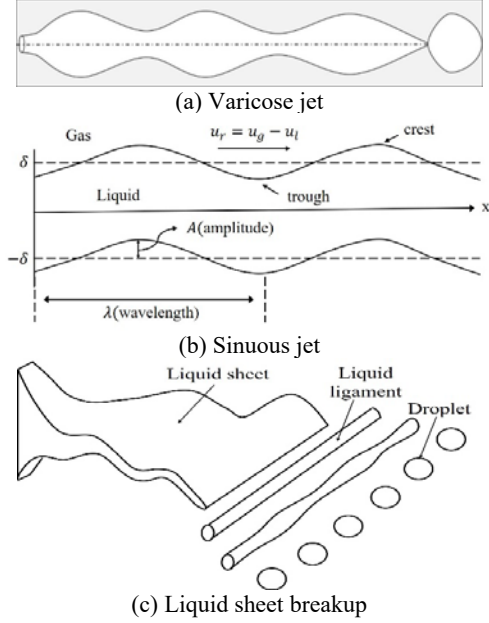


Fig. 1. Schematics of liquid jet and sheet

3.2. Modelling

In this study, based on the observation results of the visualization experiments, the droplet entrainment rate of the core liquid jet and the liquid sheet was modeled using some correlations[2] and instability analysis[13]. The entrainment rate is defined as follows.

$$m_E = \frac{V_{entr} \rho_l}{A_f \tau_w} \quad (1)$$

where ρ_l and A_f are liquid density and flow area, respectively. To obtain m_E , the volume of entrained droplets, V_{entr} , and the breakup time τ_w were modeled. In the case of the core liquid jet breakup in the inverted annular flow, it is assumed that the droplets detached by the wavelength of the wave, λ , based on the experiment of Ishii and Jarlais[2]. And, assuming that there is a core liquid jet per subchannel, V_{entr} is defined as follows.

$$V_{entr} = N_{jet} \frac{\pi}{4} D_{jet}^2 \lambda \quad (2)$$

In the above equation, N_{jet} and D_{jet} are the number of jets and the jet diameter, respectively. τ_w is defined as the breakup length L_B divided by the velocity of the liquid jet.

$$\tau_w = \frac{L_B}{u_l} \quad (3)$$

λ and L_B in Eqs. 2 and 3 are calculated using the correlations proposed by Ishii and Jarlais[2]. Table II shows the correlations for the varicose jet and the sinuous jet.

The experimental result that the liquid sheet is generated from the crest of the roll wave[2] and the result of instability analysis for the liquid sheet of Senecal[13] were introduced to derive the droplet entrainment on the liquid sheet. It is assumed that the liquid sheet is uniformly located near the heating surface. The correlations for the liquid sheet breakup are summarized in Table III.

The droplet entrainment model was applied as shown in Table IV based on the post-dryout regime map of TRACE code[14]. The study of Ishii and Denten [4] showed that the agitated region existed up to about 0.85 void fraction. Based on this, conditions of void fraction from 0.6, which is the transition criteria for the inverted slug, to 0.85 are considered as the agitated regime. When the void fraction is 0.85 or more, it is considered as a dispersed droplet flow. In this flow condition, the assumption that all the continuous liquid phases become droplets was applied, and so the droplet entrainment rate was defined as $m_E = \alpha_l \rho_l u_l$.

Table II: Correlations for varicose and sinuous jet

Correlations for varicose jet	
$\lambda = 5.8 D_{jet}$	
$D_{jet} = \sqrt{\frac{4 A_{sub} \alpha_l}{\pi}}$	$N_{jet} = \frac{A_f}{A_{sub}}$
$L_B = 480 \text{Re}_j^{-0.53} \text{We}_j^{0.5} D_{jet}$	
Correlations for sinuous jet	
$\lambda = 7.6 \sqrt{\frac{\alpha_g^2}{\text{We}_{g,rel}}} D_{jet}$	
$D_{jet} = \sqrt{\frac{4 A_{sub} \alpha_l}{\pi}}$	$N_{jet} = \frac{A_f}{A_{sub}}$
$L_B = 685 \text{Re}_j^{-0.53} \text{We}_j^{0.5} D_{jet} \left(\frac{\alpha_g^2}{\text{We}_{g,rel}} \right)^{0.645}$	

Table III: Correlations for the liquid sheet

$V_{entr} = \frac{\lambda_s}{2} \frac{\lambda_{rw}}{2} P_h$	
$\lambda_s = \frac{3\pi\sigma}{\rho_g u_r^2}$ [13]	$\lambda_{rw} = 7.6 \sqrt{\frac{\alpha_g^2}{\text{We}_{g,rel}}} D_{jet}$
$\tau_w = \frac{1}{w_{r,max}} \ln\left(\frac{a}{a_0}\right)$ [13]	
$w_{r,max} = \sqrt{\frac{4\rho_g^3 u_r^6}{27\sigma^2 \rho_l}}$, $\ln\left(\frac{a}{a_0}\right) = 12$	

Table IV: Application of the droplet entrainment model for flow regime

	Flow regime	Entrainment model	α_g
1.0	Dispersed droplet	$m_E = \alpha_l \rho_l u_l $	0.85
0.9			
0.6	Inverted slug (Transition)	Core liquid jet & Liquid sheet	
0.0	Inverted annular	Core liquid jet & Liquid sheet or Sinuous jet or Varicose jet	

4. Model assessment

4.1. Reflood tests selected for model assessment

The FLECHT SEASET and FEBA, which are representative reflood heat transfer experiments, were used to evaluate the existing models and the new model. The experimental data used for model assessment are summarized in Tables V and VI. For the CUPID calculation, test sections of both experiments were simulated in one dimension.

Table V: The selected FEBA test conditions

Test No.	Pressure (bar)	Inlet velocity (m/s)	Inlet temp. (°C)	
			0-30s	End
210	4.2	0.028	48	39
221	6.1	0.028	51	37
223	2.2	0.038	44	36
220	6.2	0.038	49	37
218	2.1	0.058	42	37
214	4.1	0.058	45	37
222	6.2	0.058	43	36

4.2. Assessment results

The existing droplet entrainment models and the new model were implemented into the CUPID code and the models were assessed using the FEBA and FLECHT SEASET reflood tests. When evaluating the models, the peak clad temperature (PCT) of each test condition and the quenching time (QT) at the location where the PCT occurred were compared with the calculation results. When comparing PCT, the highest temperature measured in the experiment was compared to the calculated temperature at the same position. QT was defined as the time at which the greatest change in clad temperature per unit time. Tables VII ~ X summarize the PCT error and QT error for each model. To compare the prediction performance of each model, the mean

absolute error(MAE) is shown in the bottom row of each table. For the FEBA experiment, the new model shows the smallest error in both PCT and QT(Tables VII and VIII). For the FLECHT SEASET experiment, the new model yields the smallest PCT error(Table XI). In the case of QT, the new model shows a slightly larger error than the other models(Table X). However, from the overall perspective, it can be said that the new model best predicts PCT and QT.

Table VI: The selected FLECHT SEASET test conditions

Test No.	Pressure (bar)	Inlet velocity (m/s)	Coolant temp. (°C)
30817	2.7	0.039	53
31021	2.8	0.039	52
31108	1.3	0.079	33
31203	2.8	0.038	52
31302	2.8	0.077	52
31504	2.8	0.024	51
31701	2.8	0.155	53
31805	2.8	0.021	51
31922	1.4	0.027	35
32013	4.1	0.026	66
34006	2.7	0.015	51
34209	1.4	0.027	32
34524	2.8	0.040	52
34610	1.4	0.021	32

Table VII: PCT error for the FEBA tests

Test No.	PCT error (K)				
	New model	COBRA-TF	Yonamoto	Holowach	CATHARE
210	8.30	23.50	-25.10	-30.40	-28.70
214	-23.33	-19.53	-15.33	-15.33	-11.93
218	-13.32	-19.02	-29.62	-23.92	-20.62
220	-38.93	-41.43	-34.03	-35.73	-36.73
221	-15.92	-23.62	-9.32	-12.62	-12.62
222	-11.71	-1.81	4.09	5.49	4.99
223	0.94	-8.56	-15.06	-16.16	-8.76
MAE	16.06	19.64	18.94	19.95	17.76

Table VIII: QT error for the FEBA tests

Test No.	QT error (s)				
	New model	COBRA-TF	Yonamoto	Holowach	CATHARE
210	29.08	44.58	-22.92	-31.42	-47.92
214	10.75	-8.75	-25.75	-30.75	-41.75
218	8.40	-51.60	-65.60	-60.10	-65.10
220	4.20	-6.30	-24.30	-37.30	-42.80
221	35.90	38.40	24.90	-4.60	-20.60
222	17.10	-5.90	-28.40	-30.90	-38.40
223	14.15	-19.35	-73.85	-58.85	-76.35
MAE	17.08	24.98	37.96	36.27	47.56

Table XI: PCT error for the FLECHT SEASET tests

Test No.	PCT error (K)				
	New model	COBRA-TF	Yonomoto	Holowach	CATHARE
30817	11.87	-0.63	-20.63	11.87	-11.53
31021	-36.03	-35.33	-35.33	-36.03	-31.43
31108	-4.01	-25.01	-19.41	-4.01	-13.91
31203	1.62	4.72	1.52	5.22	13.32
31302	-17.05	-22.35	-16.25	-17.05	-10.25
31504	43.57	32.77	19.17	39.07	52.37
31701	-58.74	-55.54	-55.84	-58.64	-54.24
31805	-5.05	-2.85	-20.25	-16.65	10.95
31922	-10.78	-12.38	-7.78	-16.78	-2.48
32013	-17.62	-17.02	-21.42	-25.52	-9.52
34006	-85.72	-85.02	-97.02	-82.42	-80.82
34209	13.03	19.73	0.33	13.03	38.03
34524	-27.02	-37.42	-59.62	-27.02	-43.82
34610	-2.76	-1.26	-15.16	-12.86	2.94
MAE	23.92	25.14	27.84	26.15	26.83

Table X: QT error for the FLECHT SEASET tests

Test No.	QT error (s)				
	New model	COBRA-TF	Yonomoto	Holowach	CATHARE
30817	-29.71	-36.21	-42.21	-29.71	-38.71
31021	-10.45	-7.45	-9.45	-10.45	-12.45
31108	45.95	26.45	26.95	45.95	24.95
31203	-11.92	-9.92	-17.92	-12.42	-17.92
31302	10.85	1.85	2.35	10.85	5.35
31504	-13.48	-14.98	-22.98	-11.98	-15.98
31701	39.65	47.15	47.15	45.15	41.15
31805	-35.83	-44.33	-57.33	-40.83	-36.33
31922	6.47	4.47	-5.53	7.97	4.97
32013	10.42	9.42	2.42	6.42	5.92
34006	-14.04	-12.04	-19.54	-7.54	-12.04
34209	-38.05	-40.55	-57.55	-38.05	-35.55
34524	17.93	18.43	7.43	17.93	9.93
34610	6.50	6.00	-1.00	5.50	7.00
MAE	20.80	19.95	22.84	20.77	19.16

5. Conclusions

In this paper, the droplet entrainment phenomena during a reflux phase of a large-break LOCA in a PWR was mechanistically modeled. We confirmed the existing droplet entrainment models applicable to the downstream of the QF did not properly reflect the actual entrainment phenomena. To complement this, the results of the visualization experiments for the post-dryout regime were used. Through the experiments, the entrainment phenomena on the core liquid jet and liquid sheet were shown, and these were modeled using instability analysis and correlations. The CUPID calculations were carried out for 14 tests of the FLECHT SEASET and 7 tests of the FEBA to evaluate

the existing droplet entrainment models and the new model. The results of the assessment show that the new model can predict PCT and QT better than the existing models.

Acknowledgements

This research was supported by the National Research Foundation (NRF) grant funded by the Ministry of Science, and ICT of the Korean government (Grant code 2017M2A8A4015059)

REFERENCES

- [1] G. De Jarlais, M. Ishii, and J. Linehan. Hydrodynamic stability of inverted annular flow in an adiabatic simulation, *Journal of heat transfer*, Vol. 108, pp. 84-92, 1986.
- [2] M. Ishii, and G. De Jarlais. Flow regime transition and interfacial characteristics of inverted annular flow, *Nuclear engineering and design*, Vol. 95, pp. 171-184, 1986.
- [3] M. Ishii, and G. De Jarlais, Flow visualization study of inverted annular flow of post dryout heat transfer region, *Nuclear Engineering and Design*, Vol. 99, pp. 187-199, 1987.
- [4] M. Ishii, and James P. Denten. Two-phase flow characteristic of inverted bubbly, slug and annular flow in post-critical heat flux region, *Nuclear Engineering and Design* Vol. 121, No. 3, pp. 349-366, 1990.
- [5] I. Babelli, S.T. Revankar, and M. Ishii, Flow visualization study of post-critical heat flux in inverted flow, *Nuclear engineering and design*, Vol. 146, No. 1-3, pp. 15-24, 1994.
- [6] R.K. Salko, and M.N. Avramova, COBRA-TF Subchannel Thermal-Hydraulics Code (CTF) Theory Manual–Revision 0, CASL-U-2015-0054, 2015.
- [7] T. Yonomoto, A study of entrainment at a break and in the core during SBLOCA in PWR, JAERI-RESEARCH-96-024. Japan Atomic Energy Research Institute, 1996.
- [8] M.J. Holowach, et al., Modeling of droplet entrainment phenomena at a quench front, *Int. J. Heat Fluid Flow*, Vol. 24, pp. 902-918, 2003.
- [9] M. Valette, et al., Revisiting large break LOCA with the CATHARE-3 three field model, *Nuclear Engineering and Design*, Vol. 241, pp. 4487-4496, 2001.
- [10] J.J. Jeong, et al., The CUPID code development and assessment strategy, *Nucl. Eng. Technol.*, Vol. 42, No. 6, pp. 636-655, 2010.
- [11] N. Lee, et al., PWR FLECHT SEASET unblocked bundle, forced and gravity reflux task data evaluation and analysis report, EPRI NP-2013/NUREG CR-2256/WCAP 9891, 1982.
- [12] P. Ihle, and K. Rust, FEBA-Flooding Experiments with Blocked Arrays Data Report 1, Test Series I through IV, Kernforschungszentrum Karlsruhe, 1984.
- [13] P.K. Senecal, et al., Modeling high-speed viscous liquid sheet atomization, *International Journal of Multiphase Flow*, Vol. 25, pp. 1073-1097, 1999.
- [14] USNRC, TRACE V5.0 Theory Manual, Field Equations, Solution Methods, and Physical Models, United States Nucl. Regul. Comm, 2010.